Title: Reversible S-Nitrosylation in an Engineered Azurin

Authors:

Shiliang Tian[1], Jing Liu[1], Ryan E. Cowley[2], Parisa Hosseinzadeh[3], Nicholas M. Marshall[1], Yang Yu[4], Howard Robinson[5], Mark J. Nilges[1], Ninian J. Blackburn[6,*], Edward I. Solomon[2,*] and Yi Lu[1,3,4,*]

Author affiliations:
[1]Department of Chemistry, [3]Department of Biochemistry, [4]Center of Biophysics and Computational Biology, University of Illinois at Urbana-Champaign, 600 South Mathews Avenue, Urbana, Illinois 61801, USA, [2]Department of Chemistry, Stanford University, Stanford, California 94305, USA, [5]Department of Biology, Brookhaven National Laboratory, Upton, New York 11973, USA, [6]Institute of Environmental Health, Oregon Health & Sciences University, Portland, Oregon 97239, USA. [*]e-mail: yi-lu@illinois.edu; Edward.Solomon@stanford.edu; blackbni@ohsu.edu.

Reversible S-Nitrosylation in an Engineered Azurin

Abstract

S-nitrosothiols are known as reagents for NO storage and transportation, and as regulators in many physiological processes. While the S-nitrosylation catalyzed by heme proteins is well known, no direct evidence of S-nitrosylation in copper proteins has been reported. Here we report reversible insertion of NO into a copper-thiolate bond in an engineered copper center in *Pseudomonas aeruginosa* azurin by rational design of the primary coordination sphere and tuning its reduction potential via deleting a hydrogen bond in the secondary coordination sphere. The results not only provide the first direct evidence of S-nitrosylation of Cu(II)-bound cysteine within metalloproteins, but also shed light on the reaction mechanism and structural features responsible for stabilizing the elusive Cu(I)-S(Cys)NO species. The fast, efficient, and reversible S-nitrosylation reaction is used to demonstrate its ability to prevent NO inhibition of cytochrome bo_3 oxidase activity by competing for NO binding with the native enzyme under physiologically relevant conditions.

Introduction

S-nitrosylation, the covalent attachment of nitric oxide (NO) to the thiol side chain of cysteine, has emerged as an important pathway for dynamic post-translational regulation of many classes of proteins involved in important functions such as blood flow regulation,[1] muscle contraction,[2] cellular trafficking,[3] and apoptosis regulation.[4] Dysregulated S-nitrosylation has been implicated in a variety of diseases, including cancer, diabetes, and neurodegenerative disorders.[5] Although it is widely accepted that the S-nitrosylation occurs *in vivo*, the mechanisms by which nitrosothiols (RSNOs) are formed and removed are unclear.[6] S-nitrosylation occurs via one-electron oxidation of the initial complex between NO and a thiol. Thus, in the absence of an electron acceptor such as O_2 or a redox-active metal ion, the nitrosothiol does not form. Because the S-nitrosylation that occurs in cells is often enhanced under anaerobic conditions, O_2 is not absolutely required for the process.[7] Therefore, redox-active metalloproteins likely play a key role in promoting the S-nitrosylation reactions by using the metal ion as the electron acceptor. However, the current chemical knowledge of this modification is largely limited to the cases associated with heme proteins when the heme is in close proximity to the target thiol.[8-12]

While the S-nitrosylation catalyzed by heme proteins is well known, the same process promoted by copper in proteins is rare in the literature, even though the latter can play equally important roles in many redox processes in biology as heme proteins. Copper-zinc superoxide dismutase (SOD) is reported to increase the yield of S-nitrosohemoglobin and nitrosylated hemes by eliminating superoxide[8] or by facilitating the transfer of NO from S-nitroso-glutathione (GSNO) to Cysβ93 of oxyhemoglobin in concentrated solutions of the protein.[13] The Cu(II)-containing protein ceruloplasmin is also shown to catalyze S-nitrosylation of heparan-sulphate proteoglycan, glypican-1,[14] as well as the formation of GSNO from NO.[15] However, a more recent study contradicted this finding and showed that depletion or supplementation of ceruloplasmin in plasma failed to alter the levels of plasma nitrosothiol.[16] Instead, NO_2^- was observed as the major product of the reaction between NO and ceruloplasmin. It is thus proposed that the Cu(II) in ceruloplasmin can oxidize NO to NO^+, which would immediately react with water to form NO_2^-. In addition, the S-nitrosylation of bovine serum albumin and glutathione mediated by free copper ion has been shown *in vitro*.[17] Since the level of free copper ion is rigorously regulated *in vivo*,

such a free copper catalyzed S-nitrosylation observed *in vitro* is unlikely to occur *in vivo*.[18] In contrast, copper ions are outstanding catalysts for RS-NO cleavage – this makes it inherently challenging to observe RS-NO bond formation at Cu sites.[19,20]

It has been reported that type 1 blue copper (T1Cu) proteins and multicopper oxidases (MCOs) can react with NO, with concomitant production of a reversible diamagnetic charge-transfer complex.[21-24] However, complete complex formation was only observed at very low temperatures (77 K).[23] At room temperature, only very low extent (~10 %) of complex formation was observed, even in the presence of saturating concentrations of NO.[23] As the physiological concentration of NO is in the nanomolar to sub-micromolar range,[25] the reaction between NO and either T1Cu proteins or MCOs are unlikely to be physiologically relevant.

To fill a major gap of our knowledge of the chemistry behind NO reaction with copper ions and to explore if this type of chemistry can be physiologically relevant, we herein report the first direct observation of S-nitrosylation of copper-bound cysteine in an engineered red copper center in *Pseudomonas aeruginosa* azurin (Az), supported by UV-vis absorption (UV-vis), electronic paramagnetic resonance (EPR) and extended X-ray absorption fine structure (EXAFS) spectroscopic techniques. We have also elucidated the reaction mechanism and structural features responsible for stabilizing the elusive Cu(I)-S(Cys)NO species by kinetic studies and density functional theory (DFT) calculations. More importantly, we show that such a S-nitrosylation can proceed in a fast ($k = 6.7 \times 10^5$ $M^{-1}s^{-1}$) and efficient (> 90% yield) way under physiological conditions in the presence of micromolar level concentration of either protein or NO, capable of preventing NO inhibition of cytochrome bo_3 oxidase activity by competing for NO binding with a native enzyme.

Results

Design, Spectroscopic, Crystallographic and Redox Studies of an Engineered Red Copper Protein in Azurin (Cu(II)-M121H/H46EAz). To obtain direct evidence of S-nitrosylation of copper-bound cysteine in proteins, we started with wild type azurin (WTAz) from *Pseudomonas aeruginosa*, which has shown to be an excellent protein for both modeling other metalloproteins and designing novel ones,[26-30] and investigated its reaction with NO. It has been reported that WTAz reacted with NO, monitored by the decrease of the 625 nm band characteristic of the blue copper center in WTAz, and a photolabile $\{CuNO\}^{10}$ adduct was proposed to form in the process.[23,24] However, such $\{CuNO\}^{10}$ adduct was only fully formed at very low temperature (77 K).[23] At room temperature, in contrast, the intensity of the 625 nm band decreased by only ~15% under NO saturated conditions.[23] We tested the reaction of 70 μM of Cu(II)-WTAz with 5 equivalents of NO at pH 7 at room temperature and observed < 8% decrease of the 625 nm band over two hours (Supplementary Fig. 1). These results suggest that the reaction between the WTAz and NO is unlikely to be physiologically relevant.

To elucidate the structural features and reaction mechanisms that can promote S-nitrosylation in T1Cu proteins under physiological conditions, we sought to re-design WTAz to accommodate a mononuclear red copper center similar to that in nitrosocyanin,[31] because nitrosocyanin is the only member of native cupredoxins discovered to date that contains an open binding site for potential NO binding and chemical transformation. Although the biological function of nitrosocyanin has not yet been identified, preliminary evidence suggests that it is likely involved in a denitrification process and may interact with NO.[32-34] Nitrosocyanin has not been recombinantly expressed, and its expression from the native host is

cumbersome, and suffers from low yield. As a result, it requires several months of continuous growth of the native host, *Nitrosomonas europaea*, to obtain enough protein for biophysical studies. In contrast, azurin constructs are much easier to express in *E. coli* in a short time (overnight) and with high yield (~100 mg purified protein/L), amenable to spectroscopic studies and X-ray crystallography, providing us with an easily tractable model system. Given previous observations of NO interaction with T1Cu centers under non-physiological conditions, the engineered new azurins with the open binding site allow for deeper insight into the factors underlying the reactivity behind the T1Cu center and NO under physiological conditions.

Both WTAz and nitrosocyanin share high structural homology.[31] Similar to the blue copper center in WTAz, one Cys and two His ligands are found to coordinate to the copper in nitrosocyanin. A comparison of the blue and red copper centers reveals a rearrangement of the copper ligands. First, the thioether ligand in Az (Met121) is replaced with a histidine imidazolyl in nitrosocyanin (His130). Furthermore, a glutamate (Glu60) is present in nitrosocyanin in place of the His46 in Az. Based on these differences, we designed a new Az variant, M121H/H46EAz.[35] Construction, expression, and purification of apo-M121H/H46EAz was carried out following a reported procedure.[28] Titration of apo-M121H/H46EAz with $CuSO_4$ saturated at 1 equivalent Cu(II). The resulting Cu(II)-M121H/H46EAz showed a strong absorption band at 403 nm (ε = 2300 $M^{-1}cm^{-1}$) and a weak and broad band around 750 nm (Supplementary Figs 2 and 3) distinct from that of WTAz, but similar to that of nitrosocyanin. The strong absorption band around 390 nm and the weak absorption band around 720 nm in nitrosocyanin have been assigned as a $p_{\sigma(Cys)} \rightarrow$Cu(II) ligand to metal charge transfer (LMCT) and a Cu(II) d-d transition, respectively.[31,34] The fact that the 600 nm band in WTAz, assigned as $p_{\pi(Cys)} \rightarrow$Cu(II) LMCT, completely disappeared in this mutant suggests that the $d_{x^2-y^2}$ ground state of Cu(II) only overlaps with p_σ orbital of S(Cys) with minimal π interaction, similar to that in nitrosocyanin.

To obtain 3D structure of Cu(II)-M121H/H46EAz, we crystallized the protein and solved its structure. As shown in Fig. 1c, the Cu(II)-binding site adopted a more distorted tetrahedral geometry compared to WTAz (Fig. 1a). While the Cu-N(His117) distance remained similar to WTAz (2.10 Å), the distance of Cu-N(His121) was 2.40 Å, significantly shorter than the ~ 2.9 Å distance of the original Cu-S(Met121) in blue copper proteins. Consequently, the metal center is further away from the backbone carbonyl oxygen at Gly45 with a distance of 3.45 Å, longer than the ~ 3 Å in WTAz.[36] More importantly, the Cu-S(Cys112) distance is 2.28 Å, longer than the ~ 2.1 Å in blue copper proteins, but comparable to that in nitrosocyanin (2.29 Å, Fig. 1b).[36,37] The Cu-S(Cys112) distance in Cu(II)-M121HAz from *A. denitrificans* is 2.16 Å, and the elongation compared to Cu(II)-WTAz was attributed to the tighter binding of His121 to the Cu(II) center compared to Met121.[38] Therefore, the further weakening of the Cu-S(Cys112) bond in the M121H/H46EAz variant may arise from the H46E mutation and concomitant rearrangement of the first coordination sphere of the metal center. This geometric rearrangement is further supported by the observation of an exogenous water at 3.78 Å from the Cu(II) within hydrogen bonding distance of the coordinating O of Glu46 (2.56 Å) in Cu(II)-M121H/H46EAz (Fig. 1c). The presence of water and its associated hydrogen bonding network has not been observed in other cupredoxins including Cu(II)-WTAz and Cu(II)-M121HAz, but is present similarly in nitrosocyanin (Fig.1b).[37] These results suggest that we have engineered the WTAz into a red copper center structurally and spectroscopically comparable to nitrosocyanin.

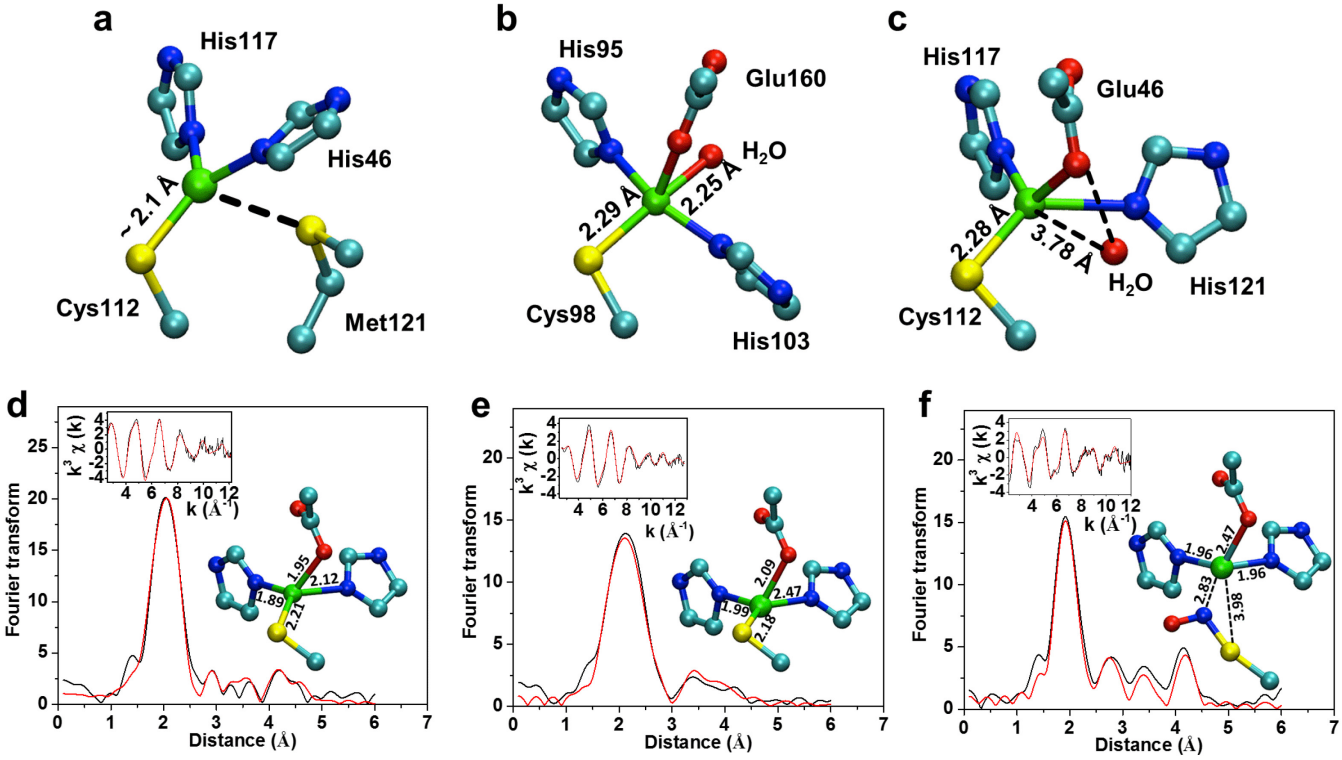

Figure 1 | **Geometries of Cu(II) binding sites and Fourier transform of EXAFS data with fitting. a**, WTAz (PDB: 4AZU), **b**, nitrosocyanin (PDB: 1IBY) and **c**, M121H/H46EAz (PDB: 4WKX). The Cu(II)-binding site in Cu(II)-M121H/H46EAz adopted a more distorted tetrahedral geometry compared to WTAz. The Cu-S(Cys112) distance in Cu(II)-M121H/H46EAz was 2.28 Å, longer than the ~ 2.1 Å in blue copper proteins, but comparable to that in nitrosocyanin (2.29 Å). An exogenous water was at 3.78 Å from the Cu(II) within hydrogen bonding distance of the coordinating O of Glu46 (2.56 Å) in Cu(II)-M121H/H46EAz. Fourier transform and EXAFS (inset) for **d**, Cu(II)-M121H/H46E/F114PAz, **e**, Cu(I)-M121H/H46E/F114PAz and **f**, NO treated Cu(II)-M121H/H46E/F114PAz. The NO treated Cu(II)-M121H/H46E/F114PAz has different EXAFS pattern from Cu(I)-M121H/H46E/F114PAz, indicating the process was not simple reduction from Cu(II) to Cu(I). The NO treated Cu(II)-M121H/H46E/F114PAz was best fitted when the Cys ligand was moved to 3.98 Å and a new N ligand was added at 2.83 Å, suggesting that the weak interaction between Cu(I) and S-nitrosothiol is through the N-atom. Experimental data are shown as solid black lines, and the simulationsas red lines. Copper atoms are green; oxygen atoms are red; sulfur atoms are yellow; nitrogen atoms are blue; carbon atoms are cyan.

The Design, Spectroscopic, and Redox studies of Cu(II)-M121H/H46E/F114PAz. Given the structural similarity between Cu(II)-M121H/H46EAz and Cu(II)-nitrosocyanin, we used cyclic voltammetry to measure E_m of Cu(II)-M121H/H46EAz. Surprisingly, its E_m = 400 mV at pH 7 is much higher than nitrosocyanin (85 mV) and is even higher than WTAz (310 mV) and M121HAz (310 mV) at pH 7.[39] This large difference in E_m prompted us to search for other mutations in the secondary coordination sphere to lower the redox potential, as demonstrated previously, and better mimic the red copper center.[40,41] Since an F114P mutation has been shown to lower the E_m of WTAz by 85 mV through deletion of one of the hydrogen bonds to Cys112 and a shift of the copper ion out of the equatorial plane,[42] we introduced the F114P mutation to M121H/H46EAz. Upon titrating Cu(II) into apo-M121H/H46E/F114PAz, the S(Cys)

→Cu(II) LMCT band was observed to shift from 403 nm to 390 nm (Fig. 2a) with a higher extinction coefficient (from ε = 2300 $M^{-1}cm^{-1}$ to 3500 $M^{-1}cm^{-1}$, Supplementary Fig. 5) compared to Cu(II)-M121H/H46EAz, consistent with the increased σ donation from S(Cys) to the Cu(II) as a result of the deletion of the hydrogen bond to Cys112. More importantly, the E_m of M121H/H46E/F114PAz was lowered to 163 mV at pH 7 and 107 mV at pH 8 (Supplementary Fig. 6), much closer to that of nitrosocyanin (85 mV at pH 7).

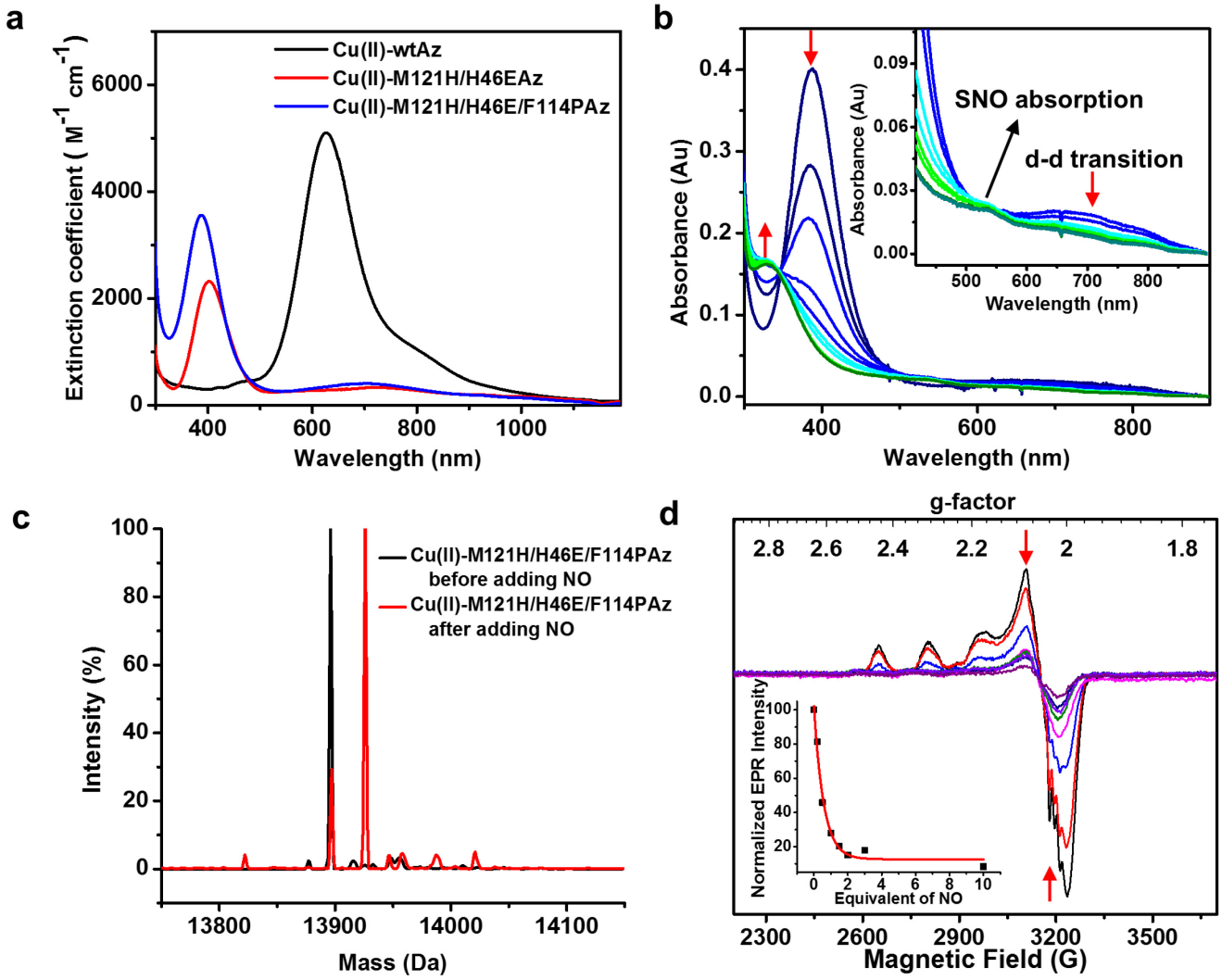

Figure 2 | UV-Vis absorption, Mass spectrometric and EPR spectroscopic characterization of S-nitrosylation in engineered red copper protein. a, The UV-Vis spectra of Cu(II)-WTAz, Cu(II)-M121H/H46EAz and Cu(II)-M121H/H46E/F114PAz. The S(Cys)→Cu(II) LMCT band of Cu(II)-M121H/H46E/F114PAz was at 390 nm, blue shifted compared to WTAz, but identical to nitrosocyanin. **b**, Kinetic UV-Vis spectra of 110 μM Cu(II)-M121H/H46E/F114PAz reacting with 1 equivalent of DEA NONOate in 50 mM Mes buffer at pH 6. A spectrum was recorded every 10 s. Upon NO addition, immediate bleaching of the 390 nm peak and an isosbestic point at 347 nm were observed. **c**, ESI-MS before (black) and after (red) NONOate addition. A mass increase of +29 Da compared to apo-M121H/H46E/F114PAz supports S-nitrosylation of the protein. **d**, X-band EPR spectra of Cu(II)-M121H/H46E/F114PAz reacting with different amounts of NO. Inset: EPR integration as a function of NO

equivalents. Decreasing signal intensity with increasing concentration of NO indicates the formation of an EPR silent species.

To further investigate the electronic structure of the Cu(II)-M121H/H46E/F114PAz, we collected its X-band EPR spectrum (Supplementary Fig. 7), which displayed *g* values of 2.237, 2.038 and 2.037 (Supplementary Table 2). Interestingly, the hyperfine coupling constants in the parallel region ($A_{//}$ = 163×10^{-4} cm^{-1}) are much larger than that of WTAz (60×10^{-4} cm^{-1}),[43] but similar to that of nitrosocyanin (144×10^{-4} cm^{-1}).[31] These results suggest that the Cu center in M121H/H46E/F114PAz is similar to red copper center in nitrosocyanin in both structural and electronic properties.

S-nitrosylation in the Engineered Red Copper Protein. To date, the function of nitrosocyanin is still unknown, but experimental evidence and genomic information suggest that nitrosocyanin could be involved in the denitrification process.[32,33] Considering the similarities between Cu(II)-M121H/H46E/F114PAz and nitrosocyanin and the observed vacant site near the metal center indicated by the distal water molecule, we treated Cu(II)-M121H/H46E/F114PAz with NO, an intermediate in the denitrification process. Upon addition of one equivalent of DEA NONOate, a NO donor which releases 1.5 NO/molecule,[44] to 110 μM of Cu(II)-M121H/H46E/F114PAz under anaerobic conditions at pH 6, immediate bleaching of the 390 nm peak was observed, suggesting disruption of the S(Cys)→Cu(II) LMCT band, which could result either from the reduction of Cu(II) to Cu(I) or modification of the coordinating S of Cys112. An isosbestic point at 347 nm indicated clean conversion to the new species with absorption around 334 nm and 540 nm (Fig. 2b), which persisted for at least one hour under anaerobic conditions, and then slowly decayed overnight at room temperature. The UV-Vis spectrum of the NO addition product is strikingly similar to that characteristic of nitrosothiols, which typically have an intense band in the 330 – 350 nm region (ε ~ 1000 $M^{-1}cm^{-1}$, assigned as $n_0 \rightarrow \pi^*$ transition) and a weak band in the 550 – 600 nm region (ε ~ 20 $M^{-1}cm^{-1}$, forbidden $n_N \rightarrow \pi^*$ transition).[19] Electrospray ionization mass spectrometry (ESI-MS) of the reaction mixture revealed a new species in ~ 80% yield with a mass increase of +29 Da compared to apo-M121H/H46E/F114PAz (Fig. 2c), further supporting S-nitrosylation of the protein. To further verify the S-nitrosylation of the protein, we performed high-resolution ESI-MS using ^{15}NO as the reactant. As shown in Supplementary Fig. 8, the isotopic pattern was shifted to higher molecular weight compared to ^{14}NO, confirming that NO was incorporated into the protein.

To further probe the S-nitrosylation process in Cu(II)-M121H/H46E/F114PAz, we collected its EPR spectra in the presence of different equivalents of NO under anaerobic conditions. The spectra showed decreasing signal intensity with increasing concentration of NO, indicating the formation of an EPR silent species (Fig. 2d). Since S-nitrosylation requires a formal one-electron oxidation of NO, the nearby Cu(II) is likely the oxidant and forms an EPR silent Cu(I)-(RSNO) product.

To obtain pseudo-first-order rate constant of this process, we measured the reaction between 50 μM of Cu(II)-M121H/H46E/F114PAz and NO in an NO-saturated buffer using a stopped-flow spectrometer (Supplementary Fig. 9). The LMCT band at 390 nm completely vanished within 10 ms, with a pseudo-first-order rate constant of 293 s^{-1}. To slow down the reaction and obtain more data points for accurate kinetic fitting, we repeated this reaction in the presence of 100 μM NO (Supplementary Fig. 9) and obtained a second-order rate constant of 6.7×10^5 $M^{-1}s^{-1}$.

Interestingly, when the freshly formed Cu(I)-S(Cys)NO species was exposed to the air at room temperature, the original LMCT band at 390 nm was recovered with a yield of ~ 66% after three hours

(Supplementary Fig. 10), indicating that the S-nitrosylation is reversible. To find out what other products were formed in this reaction, we investigated the reaction of the S-nitrosylated protein with O_2 using ESI-MS and EPR. A peak with +32 Da shift was observed in ESI-MS (Supplementary Fig. 11), suggesting that the protein was oxidized after air exposure. The MS shift is consistent with the oxidation of cysteine (Cys-SH) to cysteine sulfinic acid (Cys-SO_2H). Based on ESI-MS result, ~ 30% of the cysteine was oxidized, consistent with 66% LMCT recovery after air exposure. At the same time, a new type 2 copper signal (accounting for ~ 40% of overall Cu concentration) was observed in EPR, which displayed g values of 2.298, 2.108 and 2.037 with $A_{//} = 159 \times 10^{-4}$ cm^{-1} (Supplementary Fig. 11). We propose that Cys112 is partially oxidized by the ROS generated from the reaction between reduced Cu(I) and O_2, resulting the loss of LMCT and the formation of a new Cu(II) species. Partial recovery of the LMCT band was also consistently observed when applying vacuum to the solution containing Cu(I)-S(Cys)NO species (Supplementary Fig. 12). The slow recovery rate and low recovery ratio under air or in vacuo indicate that the reaction equilibrium highly favors the formation of S-nitrosylation product.

X-ray Absorption Spectroscopic (XAS) Studies of S-nitrosylation. Initial attempts to characterize the NO-treated Cu(II)-M121H/H46E/F114PAz sample with resonance Raman failed, probably due to the photosensitivity of the Cu-RSNO species, as S-nitrosothiols are known to be photosensitive.[20] Therefore, to further confirm the oxidation state of the copper site after S-nitrosylation and to obtain information on the ligand environment of the site, we collected Cu K-edge XAS of Cu(II)-M121H/H46E/F114PAz, Cu(I)-M121H/H46E/F114PAz, and NO-treated Cu(II)-M121H/H46E/F114PAz. To ensure the observed Cu(I) feature is not due to Cu(II) reduction upon X-ray irradiation, only one XAS spectrum was taken at each spot. As shown in Supplementary Fig. 13, an intense edge feature characteristic of Cu(I) was observed in the NO-treated Cu(II)-M121H/H46E/F114PAz sample (which was also observed in an authentic sample of Cu(I)-M121H/H46E/F114PAz prepared by adding Cu(I) to the apo-protein), indicating that the metal center was reduced to Cu(I) upon NO addition, consistent with the lack of an EPR signal (Fig. 2d). Furthermore, an XAS edge energy of 8981.29 eV (value of the peak in the first derivative of the XAS) was detected in the NO-treated Cu(II)-M121H/H46E/F114PAz sample, which was distinctly different from the edge energy of Cu(I)-M121H/H46E/F114PAz at 8980.48 eV and Cu(II)-M121H/H46E/F114PAz at 8981.54 eV (Supplementary Fig. 13).

The results of EXAFS fitting and corresponding Fourier transform are shown in Fig. 1d-f and Supplementary Table 3. The initial values for ligands and their distances were adopted from the crystal structure of Cu(II)-M121H/H46EAz. Having two His ligands at different distances significantly improved the fittings for Cu(II)-M121H/H46E/F114PAz and Cu(I)-M121H/H46E/F114PAz, consistent with the observation that the two His residues are not equivalent in the crystal structure of Cu(II)-M121H/H46EAz (Fig. 1c). The Cu-S distances of 2.21 Å and 2.18 Å were observed in Cu(II)-M121H/H46E/F114PAz (Fig. 1d) and Cu(I)-M121H/H64E/F114PAz (Fig. 1e) respectively. The NO treated Cu(II)-M121H/H46E/F114PAz was best fitted when 70% of the Cys ligand was moved to 3.98 Å and a new N ligand was added at 2.83 Å (Fig. 1f), suggesting that the weak interaction between Cu(I) and S-nitrosothiol is through the N-atom rather than the S-atom. Inclusion of O ligands in the second and third shells from Glu, NO and a presumed water molecule was used to improve the fitting. Only first shell ligands used for EXAFS fittings are shown in Supplementary Table 3.

DFT Calculations and Mechanism of Nitrosylation. Density functional theory calculations (B3LYP/TZVP) were performed to understand the mechanism of the cysteine nitrosylation using a model

of the red copper site based on the crystal structure of Cu(II)-M121H/H46EAz. Two local minima were located for the optimized Cu(II) site that differ in their core geometry and the orientation of the sulfur p orbital interacting with the Cu d_{x2-y2}. The lowest energy isomer has an S_σ ground state characteristic of red copper (Supplementary Fig. 14) that is observed experimentally by the intense observed $S_\sigma \rightarrow$ Cu LMCT at ~390 nm.[34,45] A second isomer with a blue copper S_π ground state (Supplementary Fig. 14) is higher in energy (ΔE = +2.1 kcal/mol). Similar to the red copper protein nitrosocyanin,[34] the S_σ ground state arises from two geometric effects: (1) rotation of the S(Cys)-C_β bond into the Cu equatorial plane, which orients the S_σ orbital into Cu d_{x2-y2}, and (2) the open His-Cu-His angle (138°) which orients d_{x2-y2} to overlap with S_σ. Water coordination to give five-coordinate Cu(II) was calculated to be uphill ($\Delta G°$ = +6.6 kcal/mol), consistent with the crystallography that shows the localized water adjacent to Cu(II) does not form a strong Cu-OH_2 interaction.

Two possible mechanisms for S-NO bond formation were evaluated. In the first mechanism (pathway 1 in Fig. 3), coordination of NO to Cu(II) affords a singlet five-coordinate $\{CuNO\}^{10}$ species, which is best described as Cu(I)/NO^+ due to the minor Cu character in the two unoccupied NO π* orbitals (< 20%, Supplementary Fig. 15). The Cu-NO species was not stable on the triplet spin surface; optimization invariably led to $NO^\bullet$ dissociation. Although NO coordination to Cu(II) is calculated to be unfavorable ($\Delta G°$ = +12.8 kcal/mol to singlet Cu-NO), the resulting intramolecular electrophilic attack of NO^+ on S(Cys) occurs with a low additional barrier ($\Delta G^‡$ = +5.5 kcal/mol) to give a total reaction barrier of $\Delta G^‡$ = +18.3 kcal/mol with respect to separated Cu(II) + NO reactants. The product of this electrophilic NO^+ attack is η^2-(Cys)S-NO, in which the nitrosocysteine is coordinated side-on to Cu(I) through both N and S atoms. However, this complex is thermodynamically unstable with respect to loss of the coordinated S(Cys)-NO ligand ($\Delta G°$ = -16.6 kcal/mol) to afford a trigonal Cu(I) site and free S(Cys)-NO.

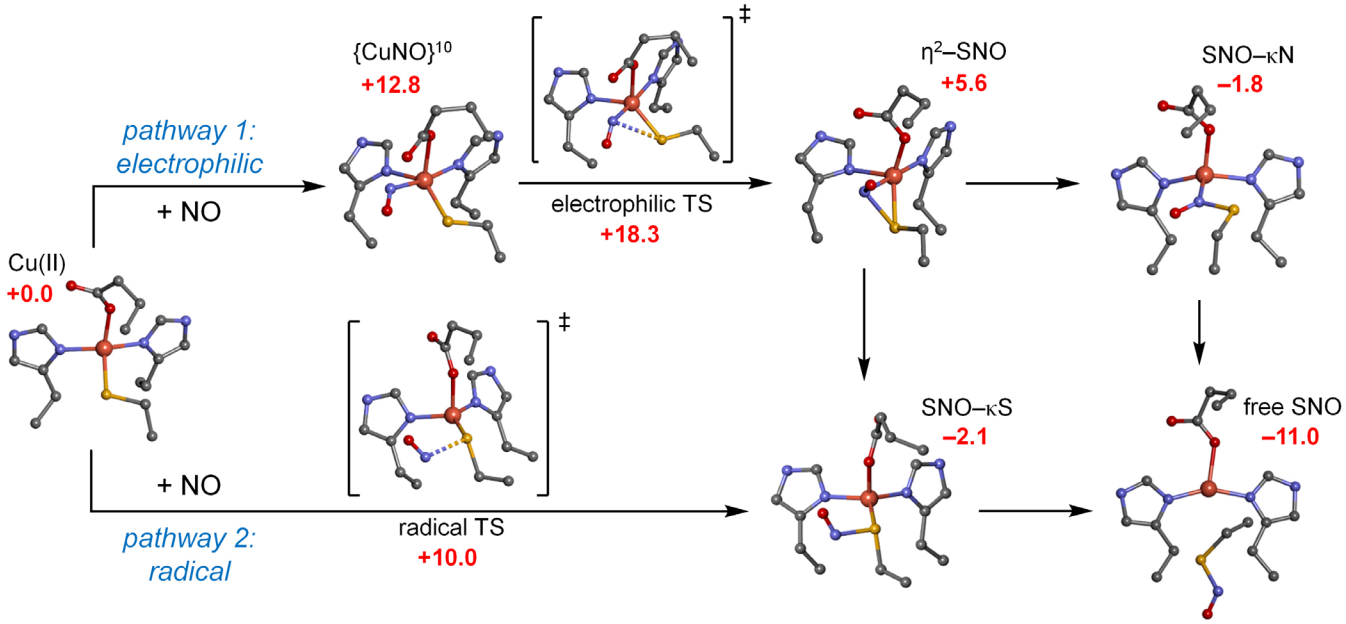

Figure 3 | Electrophilic and radical pathways for (Cys)S-NO bond formation and possible isomers of the Cu(I)/(Cys)S-NO product. In pathway 1, coordination of NO to Cu(II) affords a singlet five-coordinate $\{CuNO\}^{10}$ species. The intramolecular electrophilic attack of NO^+ on S(Cys) occurs and forms η^2-(Cys)S-NO product. In

pathway 2, NO reacts directly with S(Cys) via radical coupling without the formation of a $\{CuNO\}^{10}$ intermediate. All energies are reported as free energies (ΔG and $\Delta G^{\ddagger}$) at 298 K relative to the Cu(II) starting complex and free NO.

An alternative mechanism was also evaluated (Fig. 3, pathway 2), in which NO reacts directly with S(Cys) to avoid formation of the unfavorable $\{CuNO\}^{10}$ intermediate. In this mechanism, the high Cu-S(Cys) covalency places significant spin density (0.35 e^-) on the coordinated S in the ground state Cu(II) site (Supplementary Fig. 14), providing a pathway for direct radical coupling of S(Cys) with NO. This radical coupling reaction was evaluated by scans of decreasing S···NO distance on both the triplet and broken-symmetry (BS) singlet spin surfaces. The barrier is lowest on the BS singlet surface, proceeding with a barrier of $\Delta G^{\ddagger}$ = +10.0 kcal/mol, significantly lower than the above electrophilic mechanism ($\Delta G^{\ddagger}$ = +18.3 kcal/mol) and indicating that it is the favored pathway for S-NO bond formation. The BS singlet transition state has significant spin polarization ($<S^2>$ = 0.88) and a long S···NO distance of 2.67 Å, indicative of an early transition state. Inspection of frontier molecular orbitals along this reaction coordinate (Supplementary Figs 16 and 17) and spin density plots (Supplementary Fig. 18) show that as the NO approaches, the α-spin NO π* hole rotates to overlap with the occupied α S_π orbital, and the β-spin Cu hole polarizes towards S_π to overlap with the occupied β-spin NO π*, which results in a doubly occupied S–NO σ interaction and reduction to Cu(I). Further along the reaction coordinate (Supplementary Fig. 18), the BS wavefunction converges to an unpolarized singlet ($<S^2>$ = 0) at a S···NO distance of ~2.3 Å, and optimizes to the *S*-bound product with (Cys)S–NO = 1.90 Å. This species is also unstable with respect to loss of the coordinated S(Cys)-NO ligand, leading to the final product with S(Cys)-NO no longer bound to Cu(I) (Fig. 3, lower right). The alternative *N*-bound isomer was also calculated, but is higher energy than trigonal Cu(I) and free S(Cys)-NO ($\Delta G°$ = +9.2 kcal/mol).

The loss of the S(Cys)-NO ligand predicted by the calculations is consistent with EXAFS data that show very weak coordination of the nitrosocysteine product to Cu(I), since a coordinated S(Cys)-NO product would feature short Cu-N or Cu-S bonds (Cu-N = 2.15 Å and Cu-S = 2.36 Å for the η^2-SNO isomer, Cu-N = 2.08 Å for SNO-κN, and Cu-S = 2.37 Å for SNO-κS) that are not observed by EXAFS. The very weak ~2.8 Å Cu-N interaction observed by EXAFS is likely a result of conformational constraints of the protein backbone (which were not included in the calculations) that prevent rotation of the S(Cys)-NO away from Cu and prevent full dissociation of S(Cys)-NO, even in the "free S(Cys)-NO" structure.

DFT calculations have thus identified the most plausible mechanism for S(Cys)-NO formation is the direct radical reaction of NO with S(Cys) (Pathway 2 in Fig. 3) without formation of a $\{CuNO\}^{10}$ intermediate. Therefore, rather than oxidizing NO (to NO^+) for an electrophilic attack on S(Cys), the role of Cu(II) in this reaction is to activate S(Cys) for radical coupling with NO, a result of the high covalency of the Cu(II)-S(Cys) bond. The S-nitrosylation is calculated to be favorable ($\Delta G°$ = -11.0 kcal/mol) with a low barrier ($\Delta G^{\ddagger}$ = +10.0 kcal/mol) consistent with the observed reaction kinetics ($\Delta G^{\ddagger}$ = +9.7 kcal/mol for k_2 ~5 × 10^5 $M^{-1}s^{-1}$). The back reaction (NO release) is calculated to have a barrier of $\Delta G^{\ddagger}$ = +21.0 kcal/mol (half-life ~5 min), indicating that S-nitrosylation is slowly reversible at room temperature consistent with the experimental observation.

Competition between the engineered red copper protein and cytochrome oxidase for NO binding under physiologically relevant conditions. The high yield, fast kinetics, and preference of the S-nitrosylated product motivated us to test if the engineered red copper protein could compete with native enzymes for NO. NO is known to inhibit mitochondrial respiration by reacting with the heme-copper center in cytochrome oxidase.[46] The effect of Cu(II)-M121H/H46E/F114PAz on the NO inhibition of *E.*

coli cytochrome bo_3 oxidase activity was investigated by measuring O_2 reduction rates via a Clark-type O_2 electrode (Supplementary Fig. 19). In the presence of 5 μM NO, the O_2 reduction rate of 10 nM cytochrome bo_3 oxidase decreased by 75% (from O_2 consumption rate of 79 μmol/min to 20 μmol/min, Supplementary Fig. 19). The addition of Cu(II)-M121H/H46E/F114PAz to the above solution rescued the NO inhibition through NO sequestration (Fig. 4). 5 μM Cu(II)-M121H/H46E/F114PAz was able to rescue the inhibition of 5 μM NO on 10 nM cytochrome bo_3 oxidase by 46% (from O_2 consumption rate of 20 μmol/min to 56 μmol/min, Fig. 4 inset), recovering 71% activity of cytochrome bo_3 oxidase. The negative control experiments showed that Cu(II)-WTAz and Cu(II)-M121H/H46/F114PAz had no effect on O_2 reduction rates of cytochrome bo_3 oxidase in the absence of NO and Cu(II)-WTAz had no effect on O_2 reduction rates of cytochrome bo_3 oxidase in the presence of NO (Supplementary Fig. 20). These results demonstrated that the engineered red copper protein is capable of competing with native enzymes for NO binding.

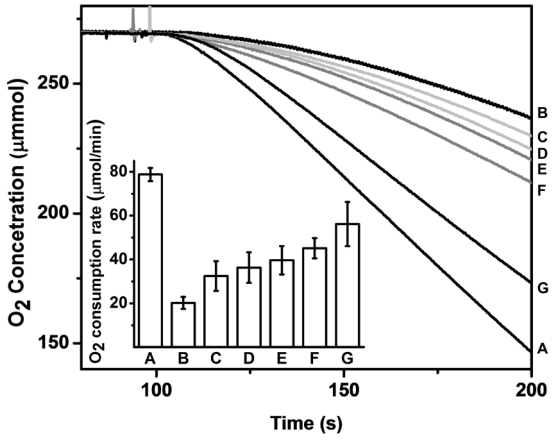

Figure 4 | Effect of Cu(II)-M121H/H46E/F114PAz on NO inhibition of *E. coli* cytochrome bo_3 oxidase. Time courses of O_2 reduction catalyzed by 10 nM cytochrome bo_3 oxidase, 100 μM ubiquinol-1 and 5 mM DTT (A) in the absence of NO, (B) in the presence of 5 μM NO, (C) 5 μM NO and 1 μM Cu(II)-M121H/H46E/F114PAz, (D) 5 μM NO and 2 μM Cu(II)-M121H/H46E/F114PAz, (E) 5 μM NO and 3 μM Cu(II)-M121H/H46E/F114PAz, (F) 5 μM NO and 4 μM Cu(II)-M121H/H46E/F114PAz, or (G) 5 μM NO and 5 μM Cu(II)-M121H/H46E/F114PAz. Inset: O_2 consumption rates derived from the slopes of initial linear regions in O_2 concentration curves. All the measurements were repeated three times and error bars indicated standard deviation. In the presence of NO, the O_2 reduction rate of cytochrome bo_3 oxidase decreased. The addition of Cu(II)-M121H/H46E/F114PAz to the above solution rescued the NO inhibition through NO sequestration, recovering 71% activity of cytochrome bo_3 oxidase.

Discussion

Cu ions are known to play important roles in regulation of NO-release from RSNOs.[19,20] For example, Cu,Zn-superoxide dismutase catalyzed the decomposition of S-nitrosoglutathione (GSNO) in the presence of GSH.[47] Cu(II) thiolate model complexes have been reported to react with S-nitrosothiols to generate NO, possibly via a RSNO-κN copper complex suggested by DFT calculations.[48] In addition, Cu(II)-doped polymers spontaneously generated NO from RSNOs, presumably via a Cu(I) intermediate.[49] Selected RSNO-Cu(I) complexes have been investigated theoretically, and it was found that coordination of the S atom to Cu(I) lengthens the S-N bond and concomitantly strengthens the N-O bond, thus promoting decomposition.[50] On the other hand, Cu(I) binding to N in the -SNO group is found to dramatically shorten and thus strengthen the S-N bond with a concomitant lengthening of the N-O bond, suggesting the

stabilization of the RSNOs versus NO release.[51] However, the barrier for interconversion of Cu(I) binding from N to S is relatively small, which makes the control of the binding modes between nitrosothiols and copper complexes difficult, and consequently Cu(I)-bound RSNO species are inherently unstable.[51] Based on the EXAFS fittings, the Cu-S distance increases from 2.18 Å in Cu(I)-M121H/H46E/F114PAz to 3.98 Å in the corresponding S-nitrosylation species, while a new N ligand was observed at 2.83 Å in the primary shell of the copper center in the S-nitrosylated species. These results indicate that the Cu(I) ion weakly interacts with the N-atom instead of S-atom of the Cys112-SNO species. This structural arrangement is consistent with the DFT calculation results, which suggests that the binding between Cu(I) and Cys112-SNO is energetically uphill. The weak Cu(I)-S(Cys)NO interaction prevents the reverse NO-releasing reaction which requires a strong Cu-S(Cys)NO bond. Therefore, the weak interaction between Cu(I) and Cys112-SNO species, together with the observed interaction with N-atom rather than S-atom, provide reasonable explanations for the stability of the RSNO species formed in our system near a Cu(I) center, allowing us to observe direct S-nitrosylation in a copper protein for the first time.

Conclusions

In summary, we have converted a blue copper center in WTAz into a red copper center that closely mimics that in nitrosocyanin first by rational design of the primary coordination sphere (M121H/H46E), and then by tuning its reduction potential via deleting a hydrogen bond in the secondary coordination sphere (F114P). The engineered red copper protein exhibits a significantly longer Cu-S(Cys) bond distance (~2.28 Å), lower reduction potential (~107 mV at pH 8) and larger hyperfine splitting in the parallel region (~160×10^{-4} cm^{-1}) as compared to blue copper proteins, and the electronic properties of the engineered protein are comparable to those of the red copper center in nitrosocyanin. Stoichiometric titration of NO to Cu(II)-M121H/H46E/F114PAz yields nearly quantitative S-nitrosylation product with concomitant reduction of the metal center with a second order rate constant of ~ 10^5 $M^{-1}s^{-1}$. The resulting S(Cys)-NO containing species shows a strong absorbance at 334 nm and a weak absorbance around 540 nm, similar to other reported RSNO species.[19] Reduction of the Cu(II) site to Cu(I) during S-nitrosylation process is confirmed by a loss of over 90% of Cu(II) signal in EPR spectrum and a shift of the Cu K-edge to lower energy. Further EXAFS fitting reveals that the Cu-S distance increases from 2.18 Å in the reduced engineered red copper protein to 3.98 Å in the S-nitrosylated species, indicating that Cu(I) interacts with N rather than S atom. DFT calculations have identified the most plausible mechanism for S(Cys)-NO formation as the direct radical reaction of NO with Cu(II)-coordinated S(Cys) enabled by the high covalency of the Cu(II)-S(Cys) bond. Our results provide the first direct evidence of S-nitrosylation of copper-bound cysteine in a protein, and show that such a reaction can prevent NO inhibition of cytochrome oxidase activity by competing for NO binding with the native enzyme.

Nitrosothiols have been known as one of the two possible naturally occurring forms for storage and delivery of NO in biological systems.[52] In our engineered red copper protein, S-nitrosylation could proceed in a fast ($k = 6.7 \times 10^5$ $M^{-1}s^{-1}$) and efficient (> 90% yield) way at room temperature at pH 7 even at micromolar protein or NO concentrations. The reaction could occur reversibly when NO could be consumed from the system by either vacuum or air. The results in Fig. 4 showed that this S-nitrosylation reaction of our engineered red copper protein could be used to rescue NO-inhibition of cytochrome oxidase activity. Such a fast, efficient and reversible S-nitrosylation under physiologically relevant conditions discovered in the engineered azurin reported here suggests that it is possible that nature may use such a reaction by copper proteins for biological functions such as NO delivery or regulation.

Materials and Methods

Crystallography. 2 μL apo-M121H/H46EAz (1.2 mM) in 100 mM NaOAc pH 5.6 buffer was mixed with 2 μL well buffer containing 25% PEG 4000, 100 mM $LiNO_3$, 10 mM $CuSO_4$ and 100 mM Tris at pH 8.0 on silica slides and equilibrated over 250 μL well buffer using hanging drop method at 4 ºC. Light green block crystals were obtained in 2-3 days. The crystals were dipped in cryo-buffer containing 70% of well buffer and 30% of glycerol before mounting and were frozen in liquid N_2 for diffraction analysis.

Collection and analysis of X-ray absorption spectra. Cu K-edge (8.9 keV) extended X-ray absorption fine structure (EXAFS) and X-ray absorption near edge structure (XANES) data were collected at the Stanford Synchrotron Radiation Lightsource (SSRL) operating at 3 GeV with currents between 100 and 80 mA. All samples were measured on beamline 9-3 using a Si 220 monochromator with crystal orientation φ = 90° and a Rh-coated mirror located upstream of the monochromator set to 13 keV to reject harmonics. A second Rh mirror downstream of the monochromator was used to focus the beam. Data were collected in fluorescence mode using a high-count-rate Canberra 100-element Ge array detector with maximum count rates below 120 kHz. A 6 μ Z-1 Ni oxide filter and Soller slit assembly were placed in front of the detector to reduce the elastic scatter peak. Six scans of a sample containing only sample buffer were collected, averaged, and subtracted from the averaged data for the protein samples to remove Z-1 Kβ fluorescence and produce a flat pre-edge baseline. The samples (80 μL) were measured as aqueous glasses (20% ethylene glycol) at 8−10 K. Energy calibration was achieved by reference to the first inflection point of a copper foil (8980.3 eV) placed between the second and third ionization chamber. The data were carefully monitored for photoreduction, and where evident, only the first spectrum of a series was included in the final average. In such cases, a new sample spot was chosen for each spectrum included in the average.

Reaction of Cu(II)-M121H/H46E/F114PAz with nitric oxide (prepared from nitric oxide saturated buffer) monitored by stopped-flow. Experiments were performed on an Applied Photophysics Ltd. (Leatherhead, U.K.) SX18.MV stopped-flow spectrometer equipped with a 256 element photodiode array detector. The instrument was prepared for anaerobic stopped-flow by rinsing out its lines several times with previously degassed buffer. Cu(II)-M121H/H46E/F114PAz solution in 50 mM MES pH6.0 buffer was degassed and equilibrated with argon on a Schlenk line. Two-syringe mixing was employed to mix equal volumes of 50 μM Cu(II)-M121H/H46E/F114PAz solution with 2 mM NO in 50 mM MES pH6.0 buffer (NO saturated) for pseudo first-order kinetics or 70 μM Cu(II)-M121H/H46E/F114PAz solution with 0.2 mM NO in 50 mM MES pH6.0 buffer (diluted from NO saturated buffer) for second-order kinetics. All reported data sets originally consisted of 200 spectra collected over 0.2 s. The integration period and minimum sampling period were both 1 ms.

Acknowledgements

This material is based on work supported by the US National Science Foundation under award no. CHE 14-13328 (Y.L.) and National Institute of Health awards DK31450 (E.I.S.) and GM054803 (N.J.B.). We thank Hirotoshi Matsumura and Pierre Moënne-Loccoz for performing initial investigation using resonance Raman spectroscopy, and Mr. Ziqiao Ding for providing *E. coli* cytochrome bo_3 oxidase, and Mr. Kevin Hwang for helpful discussions and revisions of the manuscript. Use of the Stanford Synchrotron Radiation Lightsource, SLAC National Accelerator Laboratory, is supported by the U.S.

Department of Energy, Office of Science, Office of Basic Energy Sciences under Contract No. DE-AC02-76SF00515. The SSRL Structural Molecular Biology Program is supported by the DOE Office of Biological and Environmental Research, and by the National Institutes of Health, National Institute of General Medical Sciences (including P41GM103393). The contents of this publication are solely the responsibility of the authors and do not necessarily represent the official views of NIGMS or NIH.

Correspondence and requests for materials should be addressed to Y. L., E.I.S. and N.J.B.

Author contributions

S.T., J.L., N.M.M., and Y.L. conceived and designed experiments; S.T., J.L., P.H., Y.Y. and H.R. performed experiments; S.T., R.E.C., P.H., M.J.N., N.J.B., E.I.S., and Y.L. analyzed the data; S.T., J.L., R.E.C., E.I.S. and Y.L. co-wrote the paper. All the authors discussed the results and commented on the manuscript.

References

1 Singel, D. J. & Stamler, J. S. Chemical physiology of blood flow regulation by red blood cells. *Annu. Rev. Physiol.* **67**, 99-145 (2005).

2 Xu, L., Eu, J. P., Meissner, G. & Stamler, J. S. Activation of the cardiac calcium release channel (ryanodine receptor) by poly-S-nitrosylation. *Science* **279**, 234-237 (1998).

3 Ozawa, K. *et al.* S-nitrosylation of β-arrestin regulates β-adrenergic receptor trafficking. *Mol. Cell* **31**, 395-405 (2008).

4 Benhar, M., Forrester, M. T., Hess, D. T. & Stamler, J. S. Regulated protein denitrosylation by cytosolic and mitochondrial thioredoxins. *Science* **320**, 1050-1054 (2008).

5 Anand, P. & Stamler, J. S. Enzymatic mechanisms regulating protein S-nitrosylation: Implications in health and disease. *J. Mol. Med.* **90**, 233-244 (2012).

6 Smith, B. C. & Marletta, M. A. Mechanisms of S-nitrosothiol formation and selectivity in nitric oxide signaling. *Curr. Opin. Chem. Biol.* **16**, 498-506 (2012).

7 Bosworth, C. A., Toledo, J. C., Zmijewski, J. W., Li, Q. & Lancaster, J. R. Dinitrosyliron complexes and the mechanism(s) of cellular protein nitrosothiol formation from nitric oxide. *Proc. Natl. Acad. Sci. U. S. A.* **106**, 4671-4676 (2009).

8 Gow, A. J., Luchsinger, B. P., Pawloski, J. R., Singel, D. J. & Stamler, J. S. The oxyhemoglobin reaction of nitric oxide. *Proc. Natl. Acad. Sci. U. S. A.* **96**, 9027-9032 (1999).

9 Herold, S. & Röck, G. Reactions of deoxy-, oxy-, and methemoglobin with nitrogen monoxide: Mechanistic studies of the S-nitrosothiol formation under different mixing conditions. *J. Biol. Chem.* **278**, 6623-6634 (2003).

10 Chan, N.-L., Kavanaugh, J. S., Rogers, P. H. & Arnone, A. Crystallographic analysis of the interaction of nitric oxide with quaternary-T human hemoglobin. *Biochemistry* **43**, 118-132 (2004).

11 Weichsel, A. *et al.* Heme-assisted S-nitrosation of a proximal thiolate in a nitric oxide transport protein. *Proc. Natl. Acad. Sci. U. S. A.* **102**, 594-599 (2005).

12 Schreiter, E. R., Rodríguez, M. M., Weichsel, A., Montfort, W. R. & Bonaventura, J. S-nitrosylation-induced conformational change in blackfin tuna myoglobin. *J. Biol. Chem.* **282**, 19773-19780 (2007).

13 Romeo, A. A., Capobianco, J. A. & English, A. M. Superoxide dismutase targets NO from GSNO to Cysβ93 of oxyhemoglobin in concentrated but not dilute solutions of the protein. *J. Am. Chem. Soc.* **125**, 14370-14378 (2003).

14 Mani, K., Cheng, F., Havsmark, B., David, S. & Fransson, L.-Å. Involvement of glycosylphosphatidylinositol-linked ceruloplasmin in the copper/zinc-nitric oxide-dependent degradation of glypican-1 heparan sulfate in rat C6 glioma cells. *J. Biol. Chem.* **279**, 12918-12923 (2004).
15 Inoue, K. *et al.* Nitrosothiol formation catalyzed by ceruloplasmin: Implication for cytoprotective mechanism *in vivo*. *J. Biol. Chem.* **274**, 27069-27075 (1999).
16 Shiva, S. *et al.* Ceruloplasmin is a NO oxidase and nitrite synthase that determines endocrine NO homeostasis. *Nat. Chem. Biol.* **2**, 486-493 (2006).
17 Stubauer, G., Giuffrè, A. & Sarti, P. Mechanism of S-nitrosothiol formation and degradation mediated by copper ions. *J. Biol. Chem.* **274**, 28128-28133 (1999).
18 Bertini, I., Cavallaro, G. & McGreevy, K. S. Cellular copper management—a draft user's guide. *Coord. Chem. Rev.* **254**, 506-524 (2010).
19 Williams, D. L. H. The mechanism of nitric oxide formation from S-nitrosothiols (thionitrites). *Chem. Commun.*, 1085-1091 (1996).
20 Williams, D. L. H. The chemistry of S-nitrosothiols. *Acc. Chem. Res.* **32**, 869-876 (1999).
21 Wever, R., Van Leeuwen, F. X. R. & Van Gelder, B. F. The reaction of nitric oxide with ceruloplasmin. *Biochim. Biophys. Acta* **302**, 236-239 (1973).
22 van Leeuwen, F. X. R., Wever, R., van Gelder, B. F., Avigliano, L. & Mondovi, B. The interaction of nitric oxide with ascorbate oxidase. *Biochim. Biophys. Acta* **403**, 285-291 (1975).
23 Gorren, A. C. F., de Boer, E. & Wever, R. The reaction of nitric oxide with copper proteins and the photodissociation of copper-NO complexes. *Biochim. Biophys. Acta* **916**, 38-47 (1987).
24 Ehrenstein, D., Filiaci, M., Scharf, B., Engelhard, M. & Nienhaus, G. U. Ligand binding and protein dynamics in cupredoxins. *Biochemistry* **34**, 12170-12177 (1995).
25 Hall, C. N. & Garthwaite, J. What is the real physiological NO concentration *in vivo*? *Nitric Oxide* **21**, 92-103 (2009).
26 Lancaster, K. M., DeBeer George, S., Yokoyama, K., Richards, J. H. & Gray, H. B. Type-zero copper proteins. *Nat. Chem.* **1**, 711-715 (2009).
27 Lancaster, K. M. *et al.* Outer-sphere contributions to the electronic structure of type zero copper proteins. *J. Am. Chem. Soc.* **134**, 8241-8253 (2012).
28 Sieracki, N. A. *et al.* Copper–sulfenate complex from oxidation of a cavity mutant of *Pseudomonas aeruginosa* azurin. *Proc. Natl. Acad. Sci. U. S. A.* **111**, 924-929 (2014).
29 Wilson, T. D., Yu, Y. & Lu, Y. Understanding copper-thiolate containing electron transfer centers by incorporation of unnatural amino acids and the Cu_A center into the type 1 copper protein azurin. *Coord. Chem. Rev.* **257**, 260-276 (2013).
30 Liu, J. *et al.* Redesigning the blue copper azurin into a redox-active mononuclear nonheme iron protein: Preparation and study of Fe(II)-M121E azurin. *J. Am. Chem. Soc.* **136**, 12337-12344 (2014).
31 Arciero, D. M., Pierce, B. S., Hendrich, M. P. & Hooper, A. B. Nitrosocyanin, a red cupredoxin-like protein from *Nitrosomonas europaea*. *Biochemistry* **41**, 1703-1709 (2002).
32 Chain, P. *et al.* Complete genome sequence of the ammonia-oxidizing bacterium and obligate chemolithoautotroph *Nitrosomonas europaea*. *J. Bacteriol.* **185**, 2759-2773 (2003).
33 Schmidt, I., Steenbakkers, P. J. M., op den Camp, H. J. M., Schmidt, K. & Jetten, M. S. M. Physiologic and proteomic evidence for a role of nitric oxide in biofilm formation by *Nitrosomonas europaea* and other ammonia oxidizers. *J. Bacteriol.* **186**, 2781-2788 (2004).
34 Basumallick, L. *et al.* Spectroscopic and density functional studies of the red copper site in nitrosocyanin: Role of the protein in determining active site geometric and electronic structure. *J. Am. Chem. Soc.* **127**, 3531-3544 (2005).
35 Holm, L. & Rosenström, P. Dali server: Conservation mapping in 3D. *Nucleic Acids Res.* **38**, 545-549 (2010).
36 Gray, H. B., Malmström, B. G. & Williams, R. J. Copper coordination in blue proteins. *J. Biol. Inorg. Chem.* **5**, 551-559 (2000).

37 Lieberman, R. L., Arciero, D. M., Hooper, A. B. & Rosenzweig, A. C. Crystal structure of a novel red copper protein from *Nitrosomonas europaea*. *Biochemistry* **40**, 5674-5681 (2001).

38 Messerschmidt, A. *et al.* Rack-induced metal binding vs. Flexibility: Met121His azurin crystal structures at different pH. *Proc. Natl. Acad. Sci. U. S. A.* **95**, 3443-3448 (1998).

39 Pascher, T., Karlsson, B. G., Nordling, M., Malmström, B. G. & Vänngård, T. Reduction potentials and their pH dependence in site-directed-mutant forms of azurin from *Pseudomonas aeruginosa*. *Eur. J. Biochem.* **212**, 289-296 (1993).

40 Marshall, N. M. *et al.* Rationally tuning the reduction potential of a single cupredoxin beyond the natural range. *Nature* **462**, 113-116 (2009).

41 Hosseinzadeh, P. *et al.* Design of a single protein that spans the entire 2-V range of physiological redox potentials. *Proc. Natl. Acad. Sci. U. S. A.* **113**, 262-267 (2016).

42 Yanagisawa, S., Banfield, M. J. & Dennison, C. The role of hydrogen bonding at the active site of a cupredoxin: The Phe114Pro azurin variant. *Biochemistry* **45**, 8812-8822 (2006).

43 Lu, Y. in *Comprehensive coordination chemistry II* (eds Jon A. McCleverty & Thomas J. Meyer) 91-122 (Pergamon, 2003).

44 Keefer, L. K., Nims, R. W., Davies, K. M. & Wink, D. A. in *Methods enzymol.* Vol. 268 (ed Packer Lester) 281-293 (Academic Press, 1996).

45 Solomon, E. I. Spectroscopic methods in bioinorganic chemistry: Blue to green to red copper sites. *Inorg. Chem.* **45**, 8012-8025 (2006).

46 Sarti, P. *et al.* Nitric oxide and cytochrome *c* oxidase: Mechanisms of inhibition and NO degradation. *Biochem. Biophys. Res. Commun.* **274**, 183-187 (2000).

47 Jourd'heuil, D., Laroux, F. S., Miles, A. M., Wink, D. A. & Grisham, M. B. Effect of superoxide dismutase on the stability of S-nitrosothiols. *Arch. Biochem. Biophys.* **361**, 323-330 (1999).

48 Zhang, S., Çelebi-Ölçüm, N., Melzer, M. M., Houk, K. N. & Warren, T. H. Copper(I) nitrosyls from reaction of copper(II) thiolates with S-nitrosothiols: Mechanism of NO release from RSNOs at Cu. *J. Am. Chem. Soc.* **135**, 16746-16749 (2013).

49 Oh, B. K. & Meyerhoff, M. E. Spontaneous catalytic generation of nitric oxide from S-nitrosothiols at the surface of polymer films doped with lipophilic copper(II) complex. *J. Am. Chem. Soc.* **125**, 9552-9553 (2003).

50 Toubin, C., Yeung, D. Y. H., English, A. M. & Peslherbe, G. H. Theoretical evidence that Cu^{I} complexation promotes degradation of S-nitrosothiols. *J. Am. Chem. Soc.* **124**, 14816-14817 (2002).

51 Baciu, C., Cho, K.-B. & Gauld, J. W. Influence of Cu^{+} on the RS−NO bond dissociation energy of S-nitrosothiols. *J. Phys. Chem. B* **109**, 1334-1336 (2005).

52 Wang, P. G. *et al.* Nitric oxide donors: Chemical activities and biological applications. *Chem. Rev.* **102**, 1091-1134 (2002).